Sustained Adaptive Spectral States: Global Attraction, Nonlinear Gain, and Linked Coherent–Dissipative Response

Jeremy Rodgers

Reserved DOI: 10.5281/zenodo.23927855

everythingequation.com

3 November 2026

Abstract

A constant external input can sustain an adaptive spectral carrier whose unforced amplitudes and memory would relax. We study a finite complex amplitude coupled reciprocally to real edge memory through a positive stiffness operator. An energy-conjugate rate-port contract separates physical supplied power from a tilted Lyapunov function. Stationary memory elimination gives a Lambert-W potential whose sharp edge-curvature bound yields the sufficient condition $\mu > \chi\|L\|$, with $\chi = (2-\sqrt{3})\mathrm{e}^{-\sqrt{3}}$. Under this condition every constant complex input has one globally asymptotically stable equilibrium. The complete amplitude–memory Hessian proves local exponential stability with an explicit conservative rate, despite failure of global joint convexity. On a three-node path, a prescribed contrast input produces an exact nonlinear gain law, evaluated as 1.0529729143 for the fixed parameters. Equal-norm inputs have equal stationary supplied power while sustaining different amplitudes, memory and stored energy. Conditional coherent and dissipative generators remain proportional, while freely responding memory produces a causal kernel and distinct static and frequency responses. Matched fixed-carrier controls and independent numerical formulations verify these predictions. The resulting externally powered constitutive realization quantifies feedback beyond imposed preparation and specifies the resources needed to test its response laws.

1 From relaxing carriers to sustained adaptive states

The canonical spectral-curvature field (CSCF) framework relates coherent evolution and dissipative relaxation to a common positive carrier [Rodgers, 2026a]. A fixed carrier makes that linkage transparent, but says little about what changes the carrier or keeps a nonzero state present. Reciprocal adaptive carriers introduce a source amplitude and an evolving memory [Rodgers, 2026b]. In the positive, unforced finite model, amplitudes decay and memory returns to zero. Sustained organization therefore requires an additional energy source and a corresponding account of what the source imposes.

Here the source is a prescribed constant complex amplitude-rate input. We ask three linked questions. When does it sustain a unique stable adaptive state? Which differences from an identically driven fixed carrier arise from reciprocal feedback? Which coherent–dissipative response relations survive when the carrier itself responds? We answer these questions for one finite constitutive class. The input specifies its spatial preparation and phase. Feedback changes the resulting amplitude, memory, stiffness and probe response.

The source-to-readout distinction determines which dynamics an observation can predict. A state includes both amplitude and memory, an actuator supplies work, and a positive operator converts that state into coherent and dissipative dynamics. Retaining an amplitude or an instantaneous spectrum does not in general retain future response after a memory perturbation. This is an explicit instance of the descent and projected-dynamics issues in Shadow Theory [Rodgers, 2026c,d]: a retained observable needs a closed evolution law or a memory term, rather than an assumed autonomous law on its fibers. We derive that term directly.

Our main theorem applies to every constant complex input on a finite incidence network under one sufficient graph-curvature inequality. Its proof uses stationary memory elimination, not instantaneous memory equilibration. A three-node path then supplies exact collective and contrast controls, a nonlinear gain prediction and an equal-power comparison. The response analysis returns to the full memory dynamics. No universal microscopic origin for earlier atomic, image or Kerr profiles is inferred from this construction.

2 Source state, actuator and physical energy

2.1 Constitutive equations and units

Let $z \in \mathbb{C}^n$ and $m \in \mathbb{R}^p$. Real incidence vectors $b_e \in \mathbb{R}^n$ define

$$B_e = b_e b_e^T, \qquad L = \sum_{e=1}^{p} B_e, \qquad K(m) = \mu I + \sum_{e=1}^{p} \mathrm{e}^{m_e} B_e, \quad \mu > 0. \tag{1}$$

The baseline edge stiffness has been normalized to one. A positive baseline stiffness k_e can be absorbed by replacing b_e with $\sqrt{k_e} b_e$; L and every incidence-dependent bound then use these same scaled vectors. The amplitude metric is fixed and Euclidean. Vector norms are Euclidean and operator norms are the induced spectral norms unless specified otherwise. In particular, $K(m) \geq \mu I$ for all finite m, including on the graph's collective subspace. The stored energy and its memory gradient are

$$F(z, m) = \tfrac{1}{2} z^* K(m) z + \tfrac{\kappa}{2} |m|^2, \quad \kappa > 0, \tag{2}$$

$$(F_m)_e = \kappa m_e + \tfrac{1}{2} \mathrm{e}^{m_e} |b_e^T z|^2. \tag{3}$$

For $\gamma, \alpha, \eta > 0$, set $c = \gamma + i\alpha$. The driven equations are

$$\dot{z} = -cK(m)z + f, \qquad \dot{m} = -\eta F_m(z, m), \qquad f \in \mathbb{C}^n \text{ constant}. \tag{4}$$

No target profile is used to adjust f during evolution. Positivity of η makes the memory respond to the same energy that generates the amplitude effort. This reciprocal coupling is an added constitutive assumption.

If amplitude has units A and energy has units E, then m and b_e are dimensionless, K and μ have units E/A^2, κ has units E, f has units A/s, γ and α have units $A^2/(E\,\mathrm{s})$, and η has units $1/(E\,\mathrm{s})$. The unnormalized edge coefficients carry the units of K. Choosing scales A_0, E_0, t_0 gives dimensionless versions of these equations, with $\widetilde{f} = t_0 f / A_0$. All joint-state norms and numerical parameters below use these normalized coordinates. Mixing amplitude and memory norms before fixing their scales would give a dimensionally arbitrary rate bound.

2.2 The effort–flow input contract

Write $q = (\operatorname{Re} z, \operatorname{Im} z)^T \in \mathbb{R}^{2n}$ and set

$$K_R = \operatorname{diag}(K, K), \quad J = \begin{pmatrix} 0 & -I \\ I & 0 \end{pmatrix}, \quad G = \gamma I + \alpha J, \quad f_R = (\operatorname{Re} f, \operatorname{Im} f)^T. \tag{5}$$

Each amplitude quadrature has an active rate port. Its imposed flow is f_R and its energy-conjugate effort is $y = K_R q$. The supplied power is therefore

$$P_{\text{in}} = y^T f_R = \operatorname{Re}\left[(Kz)^* f\right]. \tag{6}$$

This is the effort–flow pairing of a dissipative port-Hamiltonian description [van der Schaft and Jeltsema, 2014]. Explicitly, for $x = (q, m)$,

$$\dot{x} = (\mathcal{J} - \mathcal{R})\nabla F + \mathcal{B} f_R, \quad \mathcal{J} = \operatorname{diag}(-\alpha J, 0), \quad \mathcal{R} = \operatorname{diag}(\gamma I, \eta I), \quad \mathcal{B} = \begin{pmatrix} I \\ 0 \end{pmatrix}, \quad y = \mathcal{B}^T \nabla F. \tag{7}$$

The skew matrix $\mathcal{J}$ contributes no energy change. Direct differentiation gives the physical balance

$$\dot{F} = -\gamma \|Kz\|^2 - \eta \|F_m\|^2 + P_{\text{in}}. \tag{8}$$

External and internal amplitude flows can cancel while positive input power offsets dissipation. The supply is prescribed outside the modeled state. It is not a finite reservoir whose depletion is included in (4). For arbitrary initial states, (6) can be negative, so the ideal actuator must also be able to absorb returned energy.

A laboratory envelope interpretation would require an independently declared clock and phase reference, a calibrated two-quadrature actuator, and measurements showing that (2) and its conjugate effort represent the relevant physical energy. An arbitrary optical pump need not obey this contract. The present equations establish a consistent open energy model, without supplying those experimental facts.

3 Global solutions and the stationary reduction

3.1 A mathematical tilt distinct from stored energy

For constant f, define $\ell = f/c$, with physical units E/A, and

$$V(z, m) = F(z, m) - \operatorname{Re}(\ell^* z). \tag{9}$$

Realification gives $f_R = G\ell_R$, so

$$\dot{q} = -GV_q, \qquad \dot{m} = -\eta V_m, \qquad \dot{V} = -\gamma \|Kz - \ell\|^2 - \eta \|F_m\|^2 . \tag{10}$$

The tilt is available for every constant input; it is not a prescription for selecting the input. V is a Lyapunov function. Its decrease is not the physical stored-energy balance of the external supply. Physical work remains governed by (8).

Proposition 3.1 (Global forward existence)**.** *For every finite network, positive $\mu, \kappa, \gamma, \eta$, any $\alpha > 0$, every constant f, and every finite initial state, (4) has a unique bounded solution for all $t \geq 0$.*

Proof. Young's inequality and $K \geq \mu I$ give

$$V \geq \tfrac{\mu}{4} \|z\|^2 + \tfrac{\kappa}{2}|m|^2 - \frac{\|\ell\|^2}{\mu}. \tag{11}$$

The smooth vector field is locally Lipschitz. By (10) its solution remains in a compact sublevel of V. Local continuation on a neighborhood of that compact set excludes finite-time escape. Uniqueness follows from local Lipschitz continuity. □

Two useful bounds do not require the attraction condition proved below. The upper right Dini derivative satisfies $D^+ \|z\| \leq -\gamma\mu \|z\| + \|f\|$, including at $z = 0$. Thus

$$\|z(t)\| \leq \mathrm{e}^{-\gamma\mu t} \|z(0)\| + \frac{\|f\|}{\gamma\mu}(1 - \mathrm{e}^{-\gamma\mu t}). \tag{12}$$

Also $\dot{m}_e < 0$ when $m_e > 0$ and $\dot{m}_e \leq 0$ at $m_e = 0$. Consequently

$$m_e(t) \leq \max\{0, m_e(0)\}, \qquad K(t) \leq \mu I + \mathrm{e}^{M_0} L, \quad M_0 = \max\{0, m_1(0), \ldots, m_p(0)\}. \tag{13}$$

3.2 Eliminating memory at stationarity

For fixed z, the memory slices have second derivatives

$$\partial^2_{m_e} F = \kappa + \tfrac{1}{2}\mathrm{e}^{m_e}|b_e^T z|^2 \geq \kappa. \tag{14}$$

They are strictly convex and coercive. Their unique minima have $m_e = -s_e$, where

$$s_e \mathrm{e}^{s_e} = \frac{|b_e^T z|^2}{2\kappa}, \qquad s_e = W_0\left(\frac{|b_e^T z|^2}{2\kappa}\right) \geq 0. \tag{15}$$

Here W_0 is the nonnegative real branch of the Lambert W function [Corless et al., 1996]. At this minimum, the edge amplitude energy is κs_e and the memory energy is $\kappa s_e^2/2$. The reduced stationary potential is

$$V_{\mathrm{eff}}(z) = \tfrac{\mu}{2} \|z\|^2 + \sum_e \kappa(s_e + s_e^2/2) - \mathrm{Re}(\ell^* z). \tag{16}$$

The implicit function theorem applies since every memory second derivative is positive. The envelope derivative of (16) is $K(m(z))z - \ell$ in real coordinates. Its critical points correspond exactly to equilibria of (4), with memory restored by (15). This equivalence concerns stationary points. Replacing $m(t)$ by $-s(z(t))$ in the dynamical equation would remove a state and change both transients and response.

3.3 Why global joint convexity is unavailable

The failed convexity route can be exposed within the same three-node model used later. Take $b_1 = (1, -1, 0)^T$, $b_2 = (0, 1, -1)^T$, $\mu = 2/5$, $\kappa = 1$, $z = (3, 0, -3)^T$ real, and $m = 0$. In the real-amplitude/memory sector the joint Hessian has blocks

$$K = \mu I + L, \qquad B = 3[b_1, b_2], \qquad H_m = \tfrac{11}{2} I. \tag{17}$$

Its Schur complement is $\mu I - (7/11)L$. For $\xi = (1, 0, -1)^T$ and $\nu = (-6/11, -6/11)^T$ the complete quadratic form is exactly $-26/55$. Imaginary perturbations are zero. The tilt has the same Hessian as F, so it does not repair this negative curvature. This fixture rules out global joint convexity for the chosen model. It motivates a stationary reduction followed by a return to the complete Hessian at equilibrium; it supplies no global Euclidean contraction theorem.

4 Sharp curvature and global attraction

Lemma 4.1 (Reduced edge curvature)**.** *Let $d \in \mathbb{C}$, $r = |d|$, $s = W_0(r^2/(2\kappa))$ and $w = \mathrm{e}^{-s}$. The two real Hessian eigenvalues of $\kappa(s + s^2/2)$ are*

$$\lambda_{\tan} = w, \qquad \lambda_{\mathrm{rad}} = w\frac{1-s}{1+s}. \tag{18}$$

Their continuous values at $r = 0$ are both one. The sharp scalar lower bound is $-\chi$, where

$$\chi = (2-\sqrt{3})\mathrm{e}^{-\sqrt{3}} = 0.0474058943568\ldots. \tag{19}$$

Proof. Implicit differentiation of $s\mathrm{e}^s = r^2/(2\kappa)$ gives $\mathrm{d}s/\mathrm{d}r = 2s/[r(1+s)]$ for $r > 0$. The edge gradient is wd; its tangential derivative is w and its radial derivative is $w + r\,\mathrm{d}w/\mathrm{d}r = w(1-s)/(1+s)$. For $s \le 1$ both are nonnegative. For $s > 1$, differentiate the magnitude of the negative radial eigenvalue:

$$\frac{\mathrm{d}}{\mathrm{d}s}\left[\mathrm{e}^{-s}\frac{s-1}{s+1}\right] = \mathrm{e}^{-s}\frac{3-s^2}{(s+1)^2}. \tag{20}$$

Its maximum is attained at $s = \sqrt{3}$ and equals χ. Every nonnegative s occurs for some r, so the scalar bound is sharp. This does not assert that all graph edges can attain their worst radial directions simultaneously. □

Pulling these two-dimensional forms back through $z \mapsto b_e^T z$ yields

$$\nabla^2 V_{\mathrm{eff}} \ge \mu I - \chi L_R \ge \delta I, \quad L_R = \mathrm{diag}(L, L), \quad \delta = \mu - \chi\,\|L\|\,. \tag{21}$$

The operator norm is the Euclidean spectral norm. Multiplicities and the collective mode are retained in L_R; no selected-mode truncation enters this bound.

Theorem 4.2 (Unique sustained state and global attraction)**.** *Assume the preceding positivity hypotheses and $\delta > 0$. For every constant $f \in \mathbb{C}^n$, (4) has exactly one equilibrium (z_*, m_*). It is globally asymptotically stable. Its amplitude obeys $\|z_*\| \le \|\ell\|/\mu$ and its memory is nonpositive.*

Proof. Equation (21) makes V_{eff} strongly convex. Its baseline quadratic and linear tilt make it coercive, so it has a unique minimizer and critical point z_*. The strictly convex memory slices restore a unique m_*. Equilibrium gives $K(m_*)z_* = \ell$, proving the amplitude bound, and (15) gives $m_* \le 0$.

For completeness, consider an arbitrary trajectory in its compact V-sublevel. The nonincreasing $V(t)$ has a finite limit by (11). Define $g = \gamma\,\|Kz - \ell\|^2 + \eta\,\|F_m\|^2$. If an omega-limit point x_0 had $g(x_0) > 0$, continuity would give a ball on which $g \ge \varepsilon > 0$. The vector field is bounded on a compact neighborhood of the trajectory. Visits to a smaller concentric ball therefore entail a fixed positive residence time in the larger ball, unless the trajectory never leaves it, which would already force $V \to -\infty$. Infinitely many visits have a subsequence of disjoint residence intervals and force an unbounded decrease of V. This contradicts its finite limit. Thus every omega-limit point has $g = 0$, which by (10) is precisely the equilibrium condition. Compactness supplies at least one such point, and uniqueness implies the whole trajectory tends to (z_*, m_*).

Finally $V(z, m) \ge V_{\mathrm{eff}}(z) \ge V_{\mathrm{eff}}(z_*) = V(z_*, m_*)$, with equality only at that state. This is a strict global minimum of a proper continuous function. On any sufficiently small sphere around it, $V - V_*$ has a positive minimum. Initial states in a suitably smaller sublevel cannot cross that sphere by (10). This proves Lyapunov stability as well as global attraction. □

The compactness argument is a direct finite-dimensional Lyapunov invariance argument [LaSalle, 1976]. It proves convergence from every initial state, not uniform global exponential decay or contraction of distances between arbitrary trajectories. The condition $\delta > 0$ is sufficient. Its failure establishes neither instability nor multistability.

5 Complete local stability and a parameter bound

At equilibrium, use $q_* = (\operatorname{Re} z_*, \operatorname{Im} z_*)^T$ and write the complete Hessian

$$\mathcal{H} = \begin{pmatrix} K_R & B \\ B^T & H_m \end{pmatrix}, \quad B_{\cdot e} = \mathrm{e}^{m_{*,e}} \operatorname{diag}(B_e, B_e) q_*, \quad H_m = \operatorname{diag}\left(\kappa + \tfrac{1}{2}\mathrm{e}^{m_{*,e}} |b_e^T z_*|^2\right). \tag{22}$$

All quantities in this section are evaluated at that equilibrium. Differentiating the stationary-memory equation gives $\mathrm{d}m/\mathrm{d}q = -H_m^{-1} B^T$, so the Schur complement is

$$S = K_R - B H_m^{-1} B^T = \nabla^2 V_{\mathrm{eff}}(z_*) \geq \delta I. \tag{23}$$

Hence $\mathcal{H} > 0$. Since the mobility is constant, the full Jacobian is

$$A_{\mathrm{full}} = -D\mathcal{H}, \qquad D = \operatorname{diag}(G, \eta I), \qquad \tfrac{1}{2}(D + D^T) = \operatorname{diag}(\gamma I, \eta I). \tag{24}$$

Partial amplitude curvature alone would not establish this result; the coupling B is essential.

Proposition 5.1 (Linear rate and nonlinear local stability)**.** *Let $\sigma = \min\{\gamma, \eta\}$ in normalized coordinates, and define*

$$\theta_0 = \frac{\|\ell\| \sqrt{\sum_e \|b_e\|^4}}{\kappa\mu}, \qquad h_0 = \frac{\min\{\delta, \kappa\}}{(1+\theta_0)^2} > 0. \tag{25}$$

Then $\mathcal{H} \geq h_0 I$. With $\|v\|_{\mathcal{H}} = (v^T \mathcal{H} v)^{1/2}$, the exact linearized evolution satisfies

$$\|v(t)\|_{\mathcal{H}} \leq \mathrm{e}^{-\sigma h_0 t} \|v(0)\|_{\mathcal{H}}, \qquad \max_{\lambda \in \operatorname{spec}(A_{\mathrm{full}})} \operatorname{Re}\lambda \leq -\sigma h_0. \tag{26}$$

The nonlinear equilibrium is locally exponentially stable. Any positive rate strictly smaller than σh_0 is valid on a sufficiently small neighborhood, with respect to the fixed equilibrium Hessian norm.

Proof. Since $m_* \leq 0$, $\|B_{\cdot e}\| \leq \|b_e\|^2 \|z_*\|$. Thus $\left\|H_m^{-1} B^T\right\| \leq \kappa^{-1} \|B\| \leq \theta_0$. Completing the square gives

$$(\xi, \nu)^T \mathcal{H} (\xi, \nu) = \xi^T S \xi + (\nu + H_m^{-1} B^T \xi)^T H_m (\nu + H_m^{-1} B^T \xi). \tag{27}$$

The inverse of this shear has norm at most $1 + \theta_0$. Equations (23) and $H_m \geq \kappa I$ prove (25). For the linear equation $\dot{v} = -D\mathcal{H}v$, set $E_v = v^T \mathcal{H} v / 2$. Then

$$\dot{E}_v = -(\mathcal{H}v)^T \operatorname{diag}(\gamma I, \eta I)(\mathcal{H}v) \leq -\sigma h_0 v^T \mathcal{H} v = -2\sigma h_0 E_v. \tag{28}$$

Integration proves the norm estimate and its spectral consequence. The smooth nonlinear vector field has remainder $O(\|v\|^2)$ around its linearization. Differentiation of the same fixed quadratic form adds $O(\|v\|^3)$, which can be bounded by $2\varepsilon E_v$ on a sufficiently small neighborhood. The resulting rate is $\sigma h_0 - \varepsilon$ for any $0 < \varepsilon < \sigma h_0$; a small invariant sublevel keeps the estimate valid. □

The exact linear estimate, the neighborhood-dependent nonlinear assertion and numerical Jacobian eigenvalues are different statements. None supplies a uniform global nonlinear exponential rate. A fixed nonzero f fixes phase, so there is no neutral phase direction. At $f = 0$, positivity of μ and κ also removes zero decay rates, even though the graph Laplacian itself has a collective zero mode.

For the path in Section 8, $\|L\| = 3$ and $\mu = 2/5$. A rationally justified margin avoids treating floating eigenvalues as certificates: $\sqrt{3} > 5/3$, $2 - \sqrt{3} < 1/3$, and the cubic exponential Taylor polynomial at $5/3$ exceeds four. Hence $\chi < 1/12$ and $\delta > 3/20$. With unit input, $|c| = \sqrt{9/5} > 1$ and $\sqrt{\sum \|b\|_e^4} = \sqrt{8} < 3$, giving $\theta_0 < 15/2$, $h_0 > 3/1445$, and

$$\sigma h_0 > 9/7225. \tag{29}$$

This bound is deliberately conservative. The scalar formula (25) evaluated numerically gives approximately 0.00393374; the complete numerical spectral abscissa is approximately -0.24.

6 What the drive imposes and feedback changes

6.1 Collective control and symmetric contrast gain

For incidence vectors $b_e^T \mathbf{1} = 0$, let $\bar{z} = n^{-1}\mathbf{1}^T z$ and similarly define $\bar{f}$. Direct projection gives

$$\bar{z}(t) = \frac{\bar{f}}{c\mu} + \left(\bar{z}(0) - \frac{\bar{f}}{c\mu}\right) \mathrm{e}^{-c\mu t}. \tag{30}$$

The identically driven fixed carrier has exactly the same mean. Uniform input, uniform initial amplitude and $m(0) = 0$ give zero edge contrasts and zero memory for all time. Sustained collective amplitude is therefore an exact control for excitation without adaptive edge organization.

For the three-node path, take

$$v = (1, 0, -1)^T/\sqrt{2}, \qquad f = av, \quad a > 0. \tag{31}$$

The signed reflection that interchanges sites 1 and 3 leaves this preparation invariant. Starting from zero, the invariant sector has $z = uv$ and equal edge memories. At equilibrium write $m_1 = m_2 = -s$. Since $Lv = v$ and $|b_e^T z|^2 = |u|^2/2$, equations (15) and $Kz = \ell$ give

$$\frac{a^2}{|c|^2} = 4\kappa s \mathrm{e}^s(\mu + \mathrm{e}^{-s})^2, \qquad u = \frac{a/c}{\mu + \mathrm{e}^{-s}}. \tag{32}$$

For $a > 0$, $s > 0$. The scalar right side is strictly increasing if $\mu > \chi$: after removing positive factors, its derivative has the sign of $\mu + \mathrm{e}^{-s}(1 - s)/(1 + s)$, positive by Lemma 4.1. It begins at zero and tends to infinity. Thus (32) independently specifies exactly one nonnegative s in this regime.

For the fixed carrier $K(0)$, $u_0 = (a/c)/(\mu + 1)$. The exact gain is

$$\mathcal{G} = \frac{|u|}{|u_0|} = \frac{\mu + 1}{\mu + \mathrm{e}^{-s}} > 1. \tag{33}$$

Both the spatial mode and its phase relative to the input are imposed. Nonzero memory, persistent softening and the extra amplitude are consequences of feedback. Equal edge strengths here do not mean absent adaptation. With the parameters below, $s = 0.07303438894\ldots$ and $\mathcal{G} = 1.0529729143\ldots$, an increase of approximately 5.30%. This is a fixed-preparation prediction, not a fitted or universal gain.

A one-port input retains both mean and contrast modes. Its unequal edge intensities can produce unequal stationary memories. The calculated one-port state below demonstrates this heterogeneity; we do not infer that every asymmetric input must produce it.

6.2 Equal stationary power and continuing work

At every equilibrium, $Kz_* = \ell$ and $F_m = 0$. Equation (6) therefore yields

$$P_* = \mathrm{Re}(\ell^* c \ell) = \gamma \|\ell\|^2 = \frac{\gamma \|f\|^2}{\gamma^2 + \alpha^2}. \tag{34}$$

The same relation holds for the fixed-carrier control. Equal-norm inputs consequently have equal stationary power under this specified port contract. They can nevertheless produce different amplitudes, memories, stored energies and responses. Stationary power alone is not an adaptive-state identifier.

Corollary 6.1 (Work required for sustained organization)**.** *Under Theorem 4.2, if $f \neq 0$ then*

$$\int_0^T P_{\mathrm{in}}(t)\,\mathrm{d}t = P_* T + o(T), \qquad P_* > 0. \tag{35}$$

Cumulative internal dissipation has the same leading growth, while stored energy converges to a finite value.

Proof. Convergence of the full state implies $P_{\mathrm{in}}(t) \to P_*$ and $F(t) \to F_*$. For any $\varepsilon > 0$, split the power integral at a time after which $|P_{\mathrm{in}} - P_*| < \varepsilon$. The finite early integral divided by T vanishes and the remaining mean error is at most ε. This proves (35). Integrating (8) transfers the same leading term to the nonnegative dissipation integral because $F(T) - F(0)$ remains bounded. □

An unrefilled supply with finite available work cannot sustain the nonzero state indefinitely. The present constant-input equations do not model depletion. Their steady states are powered dissipative states in the declared amplitude coordinates, not autonomous oscillations obtained indefinitely from finite initial energy.

7 Conditional linkage and complete feedback response

7.1 Affine propagation and time ordering

Clamp or replay one memory history $m(t)$. For that history the amplitude map is affine:

$$z(t) = U(t,0)z(0) + \int_0^t U(t,s) f\,\mathrm{d}s, \qquad \partial_t U(t,s) = -cK(t)U(t,s), \quad U(s,s) = I. \tag{36}$$

The homogeneous U is conditional on the history. It is not the derivative of the full freely adapting source with respect to an arbitrary initial amplitude. Nor may its affine column be omitted from a prediction for driven amplitude.

For $A(t) = cK(t)$, its Hermitian parts are

$$H(t) = \tfrac{1}{2}(A + A^*) = \gamma K(t), \qquad C(t) = \tfrac{1}{2i}(A - A^*) = \alpha K(t) = \frac{\alpha}{\gamma} H(t). \tag{37}$$

This is the finite conditional CSCF linkage: one positive spectral carrier supplies both rates. On any finite history interval, K is bounded; if the CSCF spectral-symbol convention requires a bounded nonnegative symbol, the linear symbol on this compact spectral range can be continued constantly beyond it. No mobility is estimated by fitting the same response that is subsequently called a test.

Let $V_c' = -i\alpha K V_c$, $V_c(0) = I$. It is unitary. Writing $U = V_c R$ gives the exact interaction picture

$$\dot{R} = -\gamma V_c^* K V_c R, \qquad R(0) = I. \tag{38}$$

For $D_c' = -\gamma K D_c$, $D_c(0) = I$, the gap-free comparison inherited from the adaptive-carrier construction [Rodgers, 2026b] is

$$\|U(T) - D_c(T)V_c(T)\| \le \gamma\alpha \int_0^T \int_0^t \|[K(t), K(s)]\| \, \mathrm{d}s \, \mathrm{d}t. \tag{39}$$

For clarity, fix t and set $Q_t(s) = [K(t), D_c(s)]$. Differentiation gives

$$\dot{Q}_t(s) = -\gamma K(s) Q_t(s) - \gamma [K(t), K(s)] D_c(s), \qquad Q_t(0) = 0. \tag{40}$$

The dissipative propagators are contractions, so $\|Q_t(t)\| \le \gamma \int_0^t \|[K(t), K(s)]\| \, \mathrm{d}s$. Next $D_c V_c$ solves the U equation with residual $i\alpha[K, D_c]V_c$. Variation of constants and contraction of U prove (39). No eigenvalue gap or eigenvector-tracking hypothesis is used.

On the path, write $w_e(t) = \mathrm{e}^{m_e(t)}$. Then

$$[K(t), K(s)] = [w_1(t)w_2(s) - w_2(t)w_1(s)][B_1, B_2], \quad \|[B_1, B_2]\| = \sqrt{3}. \tag{41}$$

The symmetric contrast sector has equal moving weights and commutes across time. A one-port transient need not commute. At the attracting equilibrium the carrier is constant and conditional factorization is exact. Transient noncommutation therefore does not establish persistent noncommuting motion or a Floquet result.

7.2 Memory kernel and transfer operators

At equilibrium, let $\xi \in \mathbb{R}^{2n}$ and $\nu \in \mathbb{R}^p$ denote amplitude and memory perturbations. An additive real rate probe $r(t)$ gives

$$\dot{\xi} = -GK_R\xi - GB\nu + r(t), \qquad \dot{\nu} = -\eta B^T \xi - \eta H_m \nu. \tag{42}$$

The fixed input f contributes no state derivative. Eliminating ν is exact and gives

$$\begin{aligned} \dot{\xi}(t) = & -GK_R\xi(t) - GB\mathrm{e}^{-\eta H_m t}\nu(0) + r(t) \\ & + \eta \int_0^t GB\mathrm{e}^{-\eta H_m (t-s)} B^T \xi(s) \, \mathrm{d}s. \end{aligned} \tag{43}$$

Even zero initial memory perturbation leaves the causal kernel. Omitting the memory state without this term loses predictive information. This gives an explicit return from a projected amplitude description to the full source-to-readout dynamics.

For zero initial perturbations, the Laplace-domain transfer from r to ξ, on the complexification of the real amplitude space, is

$$\mathcal{X}_{\mathrm{full}}(p) = \left[pI + GK_R - \eta GB(pI + \eta H_m)^{-1} B^T\right]^{-1}, \tag{44}$$

$$\mathcal{X}_{\mathrm{clamp}}(p) = (pI + GK_R)^{-1}. \tag{45}$$

These inverses exist for every $\mathrm{Re}\, p \ge 0$ under Theorem 4.2. Indeed $H_m \ge \kappa I$ makes the eliminated memory block invertible there, while Proposition 5.1 makes $pI - A_{\mathrm{full}}$ invertible. Block Gaussian elimination then makes its amplitude Schur complement in (44) invertible. For the clamp, G commutes with K_R and the complex generator has eigenvalues $-c\lambda_j(K)$, with strictly negative real parts. Thus (45) is also invertible on the closed right half-plane. This covers static response and all real-frequency probes $p = i\omega$. Elsewhere the displayed Schur formula applies only where both

the memory block and the full resolvent exist; it does not assert the displayed representation at an eliminated memory pole.

At zero frequency, (23) yields

$$\mathcal{X}_{\mathrm{full}}(0) = S^{-1}G^{-1}, \qquad \mathcal{X}_{\mathrm{clamp}}(0) = K_R^{-1}G^{-1}. \tag{46}$$

The order of factors matters. Freely responding memory changes even the static susceptibility at the same equilibrium and the same probe. Moreover, $\mathcal{H}$ need not commute with $\mathrm{diag}(J, 0)$, so full feedback response cannot generally be represented by the conditional complex-linear generator cK. Positivity and proportionality of the conditional Hermitian parts do not remove this distinction.

7.3 Observable contract and required resources

A conditional linkage test requires calibrated time, the fixed amplitude metric, independently measured mobilities, phase-sensitive access to both quadratures, and enough independent preparation columns to reconstruct the operator. For a driven experiment the affine baseline must be subtracted. Memory must be clamped or identically replayed across those columns. A free-memory kick instead probes (43) or (44). Reconstructing an instantaneous spectrum, pooling amplitude magnitudes or observing a common mean does not supply these resources. The full state, input-work record and controlled-memory probe distinguish the source from its reduced readouts.

8 Executed finite calculations and matched controls

8.1 Fixed preparations and numerical methods

The retained calculation uses the three-node path and normalized parameters

$$(\mu, \kappa, \gamma, \alpha, \eta) = (0.4, 1, 0.6, 1.2, 0.8). \tag{47}$$

The three real constant inputs, all of norm one, are $(1, 1, 1)^T/\sqrt{3}$, $(1, 0, -1)^T/\sqrt{2}$ and $(1, 0, 0)^T$. All source trajectories begin at $z = 0, m = 0$ and run to $T = 100$ with 1001 retained sample times. Each has a matched control with $K = K(0)$ under the same input and initial amplitude. The eight source coordinates comprise all six real amplitude coordinates and both memories; no collective or repeated mode is discarded. Three additional integrated coordinates record dissipated energy, supplied work and tilted loss.

DOP853 calculations use relative/absolute tolerances $10^{-10}/10^{-12}$ and a tighter repeat uses $10^{-12}/10^{-14}$. A source-derived step cap is

$$\Delta t_{\max} = \frac{1}{8|c|(\mu + \mathrm{e}^{M_0}\,\|L\|)} = 0.02507581193\ldots, \tag{48}$$

where $M_0 = 0.1$ includes the admitted second initial state. Equation (13) bounds the largest source amplitude scale; this eight-step resolution is a numerical choice, not a formal error enclosure. Independent real-gradient RK4 uses 50,000 steps of size 0.002 and compares all eight states and three ledgers. Direct eight-real-coordinate stationary roots, using the complete Hessian Jacobian, are compared with a three-real-coordinate Lambert-W root. For real inputs the latter is valid because K is real and $z_* = c^{-1}K^{-1}f$ has a common complex phase. Root tolerance is 10^{-11}.

Table 1: Stationary matched controls. Contrast norms refer to the complete amplitude with its mean removed; $\Delta w = |w_1 - w_2|$.

Input	Fixed contrast	Adaptive contrast	$\|m_*\|$	Δw	P_*
Uniform	0.0000000	0.0000000	0.0000000	0.0000000	0.3333333
Contrast	0.5323971	0.5605998	0.1032862	0.0000000	0.3333333
One port	0.3869536	0.4040033	0.0746299	0.0591111	0.3333333

Table 2: Complete equilibrium stability. The last column evaluates the conservative parameter bound, rather than fitting the numerical eigenvalues.

Input	$\lambda_{\min}(\mathcal{H})$	$\max \Re\lambda(A_{\text{full}})$	σh_0
Uniform	0.4000000	-0.2400000	0.00393374
Contrast	0.4000000	-0.2400000	0.00393374
One port	0.4000000	-0.2400000	0.00393374

The original unconstrained-step run failed one frozen criterion: uniform sampled contrast was 7.35254×10^{-8}, exceeding 10^{-9}. The exact invariant control identifies this as numerical symmetry error. Its coarse/tight difference was 6.34174×10^{-8}. Original code and outputs remain available. The cap (48) was specified and frozen before the refined outcomes, applied to all source solves, and left the original thresholds unchanged. The refined run passes all 55 frozen criteria. It is a documented post-result refinement, not an untouched validation set.

8.2 Stationary organization, power and stability

Define contrast amplitude as $\|z - \bar{z}\mathbf{1}\|$, memory size as $\|m\|$, and edge heterogeneity as $|\mathrm{e}^{m_1} - \mathrm{e}^{m_2}|$. Tables and figures here are generated from the retained numerical outputs; near-zero controls are printed at their displayed precision. The symmetric memories are both -0.07303439. The one-port memories are -0.07366282 and -0.01197548, and its edge-strength difference is 0.05911106. Stored adaptive energies are 0.69444444, 0.21425722 and 0.35254833 for uniform, contrast and one-port input, respectively. The fixed-carrier values are 0.69444444, 0.19841270 and 0.34430439. Thus equal stationary power coexists with different organization and energy. These numbers compare prescribed preparations; they do not indicate spontaneous selection of the contrast mode.

The independent scalar check uses 60-decimal arithmetic and bisection of (32) on $s \in [0, 1]$, without SciPy or a Lambert-W implementation. It reproduces (33). This is an independent arithmetic evaluation of an already inspected prediction, not a new frozen holdout or an interval certificate.

The energy ledger checks $F(t) - F(0) + \int_0^t (\gamma \|Kz\|^2 + \eta \|F_m\|^2)\mathrm{d}s - \int_0^t P_{\text{in}}\mathrm{d}s$. The tilted ledger checks $V(t) - V(0) + \int_0^t [\gamma \|Kz - \ell\|^2 + \eta \|F_m\|^2]\mathrm{d}s$. These are evaluated as separate identities. Numerical attraction from a second one-port initial state, with real amplitude $(0.4, -0.2, 0.1)$, imaginary amplitude $(0.1, 0.3, -0.2)$ and memory $(0.1, -0.15)$, gives terminal equilibrium error 4.23136×10^{-11}.

8.3 Conditional ordering and full response

Conditional propagators and their affine columns are integrated to $T = 4$ using the dense source history; the commutator quadrature samples 401 times. For the symmetric contrast preparation, the $U - D_c V_c$ gap is approximately 3.26×10^{-15}. For one-port excitation it is 4.92685×10^{-4}. Interaction-picture and affine reconstruction errors remain near numerical precision. Omitting the affine term gives large amplitude errors, approximately 0.54235 and 1.33548 respectively. The

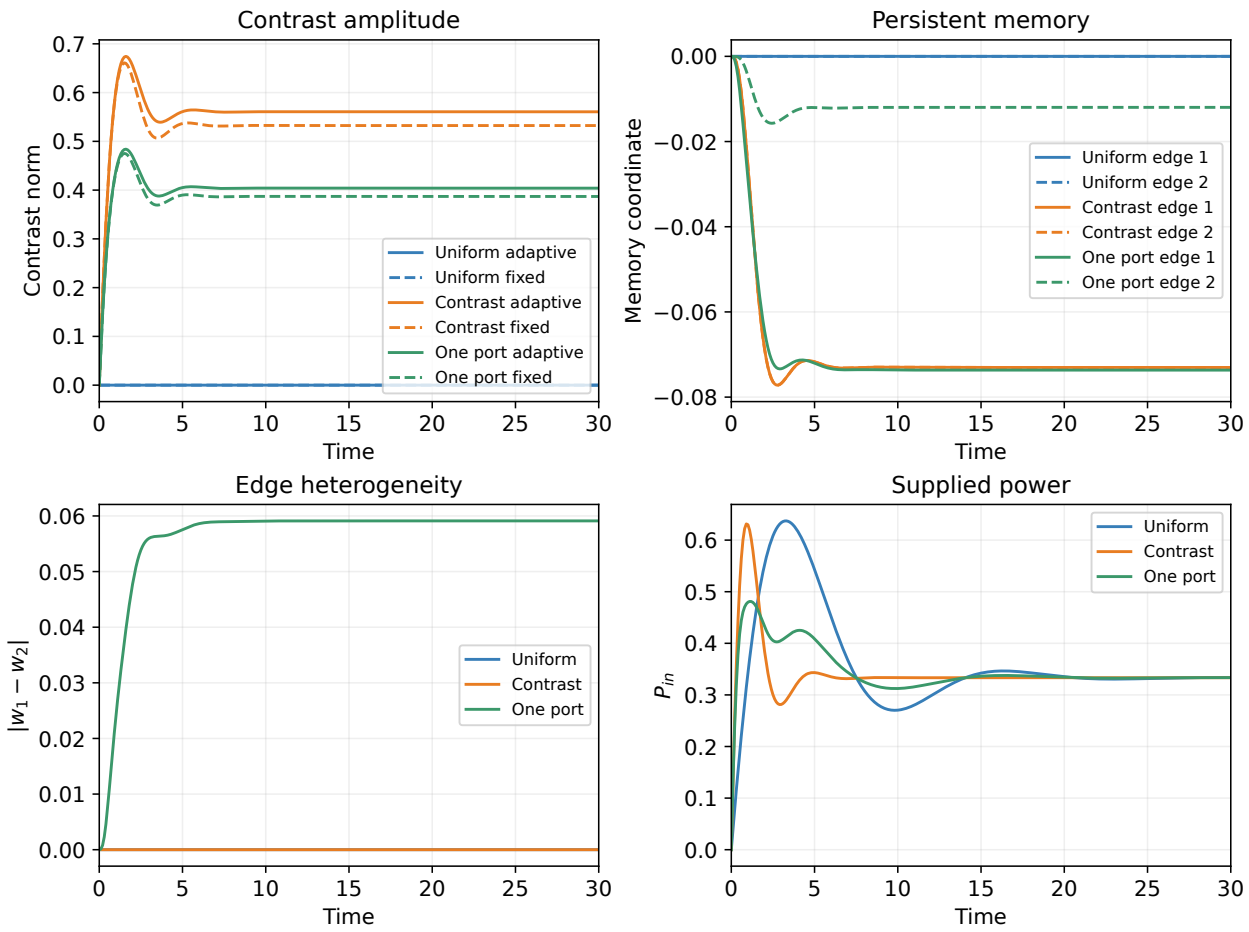


Figure 1: Identically driven adaptive and fixed-carrier controls. Contrast amplitude, both memory coordinates, edge heterogeneity and supplied power are retained. The uniform preparation sustains only the collective mode; the symmetric contrast preparation adapts with equal edges; the one-port preparation has unequal persistent memories. All powers tend to 1/3 under the declared rate-port contract.

sampled commutator double integral is a quadrature diagnostic, not a rigorous upper enclosure for (39). At the one-port equilibrium, a real amplitude-coordinate impulse is compared at time 2, and frequency transfer is evaluated at $p = 0.5i$. Static probe and Jacobian finite differences use central step 10^{-5}. The nonzero full/clamped gaps demonstrate different response contracts. The Hessian commutator norm $\|[\mathcal{H}, \mathrm{diag}(J, 0)]\| = 0.53593673$ also verifies that the complete tangent is not the conditional complex-linear dynamics.

8.4 Reproducibility and evidence scope

The accompanying verification archive contains the specifications and frozen input identities, calculation implementations, initial failed outputs, refined results, 13 trajectory arrays, the separate scalar check, generated assets, a claim-to-file map and an executable reproduction procedure. Its checker preserves discrete definitions and scientific thresholds exactly, normalizes text line endings, and checks generated table cells against the outputs of their own run at printed precision. Small residuals are judged by scientific criteria rather than incidental roundoff digits. The original failure

Table 3: Maximum diagnostics over the three preparations, except the two separately identified one-port checks. Every upper criterion retains its original strict threshold.

Diagnostic	Observed	Criterion: less than
Equilibrium residual	4.714e-16	1.0e-09
Direct/reduced root difference	3.097e-15	1.0e-08
Terminal equilibrium error	7.035e-11	2.0e-07
Coarse/tight trajectory difference	1.137e-13	2.0e-07
Physical energy ledger	1.066e-13	2.0e-07
Tilted loss ledger	3.331e-15	2.0e-07
Collective-mode formula	9.155e-16	1.0e-09
Independent real-gradient RK4	2.792e-12	2.0e-07
Second initial-state terminal error	4.231e-11	2.0e-07

Table 4: Response and conditional-history diagnostics. Transfer gaps use the operator norm; the impulse gap uses the specified first real-coordinate probe. Commutator quadrature is not a formal enclosure.

Quantity	Value
Full/clamped impulse gap	1.810309e-02
Full/clamped static transfer gap	4.678222e-02
Full/clamped frequency transfer gap	4.440963e-02
Full Jacobian finite difference	1.580285e-11
Static probe finite difference	1.825302e-11
Contrast factorization gap	3.257883e-15
Contrast interaction error	5.651507e-15
Contrast affine error	2.830524e-16
Contrast commutator quadrature	0.000000e+00
One port factorization gap	4.926845e-04
One port interaction error	5.154423e-15
One port affine error	5.926969e-16
One port commutator quadrature	2.093538e-01

and subsequent step-cap refinement remain distinguishable in the archive.

The numerical results use Python 3.12.14, NumPy 2.3.5 and SciPy 1.18.1 on Windows. Independent real-gradient RK4, direct and reduced stationary solves, and Decimal bisection check different numerical formulations of the stated model. The analytic proofs, exact negative-curvature fixture and rational stability margin establish their respective mathematical claims; floating-point trajectories, eigenvalues and quadrature do not constitute directed interval certificates. Physical validation requires the calibrated actuator and paired response measurements described in Section 7.3.

9 Consequences and focused extensions

The fixed-carrier CSCF relation survives conditionally on a controlled history, while reciprocal memory changes which state and response a drive sustains. The new all-input sufficient theorem connects a sharp scalar edge-curvature bound to global attraction on a finite network. Returning to the complete Hessian supplies local stability without the false premise of global joint convexity. The symmetric preparation converts the stationary reduction into a quantitative nonlinear gain

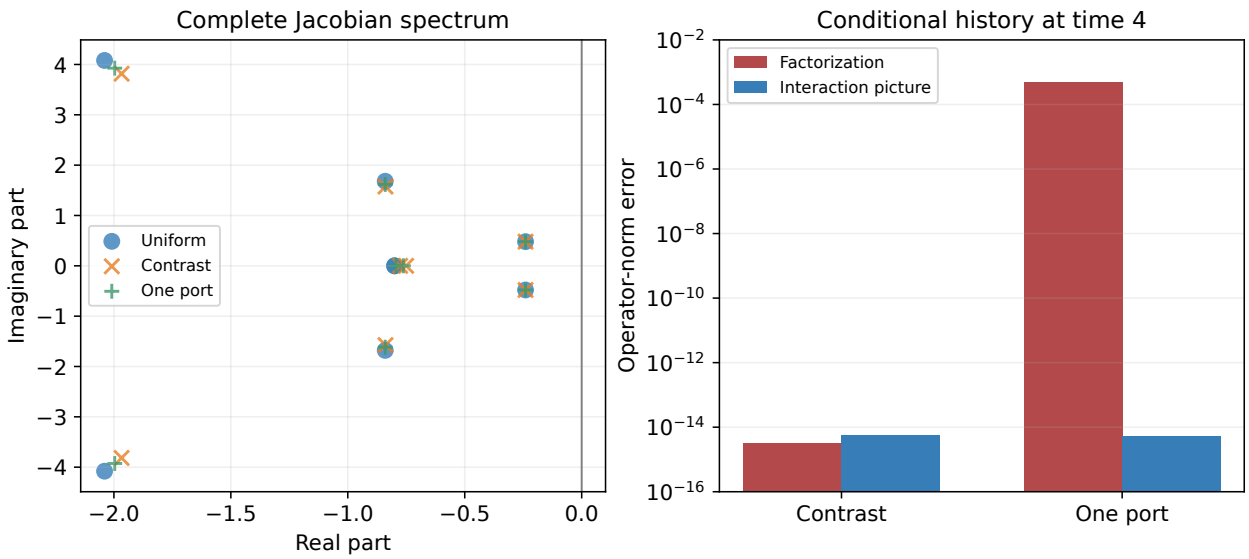


Figure 2: Complete stability and response checks. Left: all eight eigenvalues of each complete equilibrium Jacobian, retaining multiplicities. Right: transient conditional factorization and interaction-picture errors for the two nonuniform preparations. The noncommuting one-port transient relaxes to a constant carrier. Full-feedback transfer differences in Table 4 persist at equilibrium despite exact conditional factorization there.

law. The power identity and continuing-work consequence make explicit the energy resource that sustains the state.

The source-to-readout architecture also becomes experimentally discriminating. Conditional phase and decay are linked by one carrier and independently calibrated mobilities. Complete feedback response retains a causal memory kernel, measurable in a paired clamp/free-memory experiment. Neither a common mean nor equal supplied power identifies that distinction. A useful first implementation would independently calibrate the energy effort, active quadrature ports and memory state, then compare the static and phase-sensitive frequency responses under both memory constraints. Such an implementation remains future experimental work.

Time-dependent drive would require a different Lyapunov argument; finite reservoirs would add a supply state and eventual depletion; parameters outside the sufficient curvature regime require separate uniqueness and stability analysis. Continuum limits and cross-domain microscopic identification are further questions. The present result is complete within its finite constant-input class: externally sustained adaptive states have a proved attraction regime, feedback produces quantified gains beyond imposed preparation, and conditional linkage coexists with a distinct complete response.

References

Jeremy Rodgers. The canonical spectral-curvature field: A unified operator origin for coherence, dissipation, and spectral budgets, 2026a. URL https://doi.org/10.5281/zenodo.23899458. Zenodo preprint.

Jeremy Rodgers. Adaptive spectral carriers: Time ordering, reciprocal memory, and linked coherent–dissipative response, 2026b. URL https://doi.org/10.5281/zenodo.23924603. Zenodo preprint.

Jeremy Rodgers. Source readout non-equivalence: Descent and equivariant reconstruction obstructions, 2026c. URL https://doi.org/10.5281/zenodo.21369967. Zenodo preprint.

Jeremy Rodgers. Observable quotients and exact projected dynamics: Closure, memory, minimal dynamical completion, and effective field operators, 2026d. URL https://doi.org/10.5281/zenodo.21371251. Zenodo preprint.

Arjan van der Schaft and D. Jeltsema. *Port-Hamiltonian Systems Theory: An Introductory Overview*, volume 1 of *Foundations and Trends in Systems and Control*. Now Publishers, 2014. doi: 10.1561/2600000002. URL https://doi.org/10.1561/2600000002. Nos. 2–3.

Robert M. Corless, Gaston H. Gonnet, D. E. G. Hare, David J. Jeffrey, and Donald E. Knuth. On the Lambert W function. *Advances in Computational Mathematics*, 5:329–359, 1996. doi: 10.1007/BF02124750. URL https://doi.org/10.1007/BF02124750.

J. P. LaSalle. *The Stability of Dynamical Systems*, volume 25 of *CBMS-NSF Regional Conference Series in Applied Mathematics*. SIAM, 1976. doi: 10.1137/1.9781611970432. URL https://doi.org/10.1137/1.9781611970432.